Therapeutic Discovery

Molecular Cancer Therapeutics

Artesunate Induces Oxidative DNA Damage, Sustained DNA Double-Strand Breaks, and the ATM/ATR Damage Response in Cancer Cells

Nicole Berdelle[1], Teodora Nikolova[1], Steve Quiros[1], Thomas Efferth[2], and Bernd Kaina[1]

Abstract

Artesunate, the active agent from *Artemisia annua* L. used in the traditional Chinese medicine, is being applied as a first-line drug for malaria treatment, and trials are ongoing that include this drug in cancer therapy. Despite increasing interest in its therapeutic application, the mode of cell killing provoked by artesunate in human cells is unknown. Here, we show that artesunate is a powerful inducer of oxidative DNA damage, giving rise to formamidopyrimidine DNA glycosylase–sensitive sites and the formation of 8-oxoguanine and 1, *N*6-ethenoadenine. Oxidative DNA damage was induced in LN-229 human glioblastoma cells dose dependently and was paralleled by cell death executed by apoptosis and necrosis, which could be attenuated by radical scavengers such as *N*-acetyl cysteine. Oxidative DNA damage resulted in DNA double-strand breaks (DSB) as determined by γH2AX foci that colocalized with 53BP1. Upon chronic treatment with artesunate, the level of DSB continuously increased over the treatment period up to a steady-state level, which is in contrast to ionizing radiation that induced a burst of DSB followed by a decline due to their repair. Knockdown of Rad51 by short interfering RNA and inactivation of DNA-PK strongly sensitized glioma cells to artesunate. These data indicate that both homologous recombination and nonhomologous end joining are involved in the repair of artesunate-induced DSB. Artesunate provoked a DNA damage response (DDR) with phosphorylation of ATM, ATR, Chk1, and Chk2. Overall, these data revealed that artesunate induces oxidative DNA lesions and DSB that continuously increase during the treatment period and accumulate until they trigger DDR and finally tumor cell death. *Mol Cancer Ther; 10(12); 2224–33. ©2011 AACR.*

Introduction

The natural compound artemisinin, derived from *Artemisia annua* L., which has been used for centuries in the traditional Chinese medicine, and its semisynthetic derivatives artesunate (Fig. 1A) and artemether are antimalaria drugs that exert remarkable anticancer activity *in vitro* and *in vivo* (1–3). The active chemical moiety of artemisinin type compounds is an endoperoxide bridge, which is cleaved in the presence of ferrous iron by a Fenton-type reaction. This leads, in plasmodia, to the generation of reactive oxygen species (ROS), for example, hydroxyl radicals and superoxide anions (4) as well as carbon-centered radical molecules (5). In plasmodia, these reactive species were shown to alkylate proteins (5–7), which is thought to be the underlying reason of the bacteriostatic effect. Because ferrous iron is present in high amounts in erythrocytes bearing plasmodium parasites and in cancer cells, the activity towards malaria infections and cancer cells might be explained by the same biochemical mechanism. Indeed, exogenous application of iron to cancer cells in the form of transferrin or the drug Ferrosanol increased the activity of artesunate (8, 9). Furthermore, oxidative stress response genes are determinants for artesunate resistance (8, 9).

While the present model claims that protein alkylation is the cause for artesunate-induced toxicity (10), we have recently shown that artesunate is able to induce DNA damage, which is repaired by specific repair pathways (11). The molecular nature of the DNA damage induced by artesunate has not yet been identified. Because artesunate gives rise in a Fenton-type reaction to ROS, it is tempting to hypothesize that artesunate-induced ROS formation may lead to oxidative DNA damage, which ultimately accounts for the cytotoxic activity observed in cancer cells. To prove this hypothesis, we measured the formation of 8-oxoguanine (8-oxoG) and 1,*N*6-ethenoadenine (ethenoA), which are main oxidative DNA lesions, following treatment of LN-229 human glioblastoma cells with artesunate. Oxidative DNA damage, induction of DNA double-strand breaks (DSB), DNA damage

Authors' Affiliations: [1]Institute of Toxicology, University Medical Center; and [2]Institute of Pharmacy, Johannes Gutenberg University, Mainz, Germany

Corresponding Author: B. Kaina, University of Mainz, Obere Zahlbacher Str. 67, Mainz D-55131, Germany. Phone: 49-6131-17-9217; Fax: 49-6131-230506; E-mail: kaina@uni-mainz.de

doi: 10.1158/1535-7163.MCT-11-0534

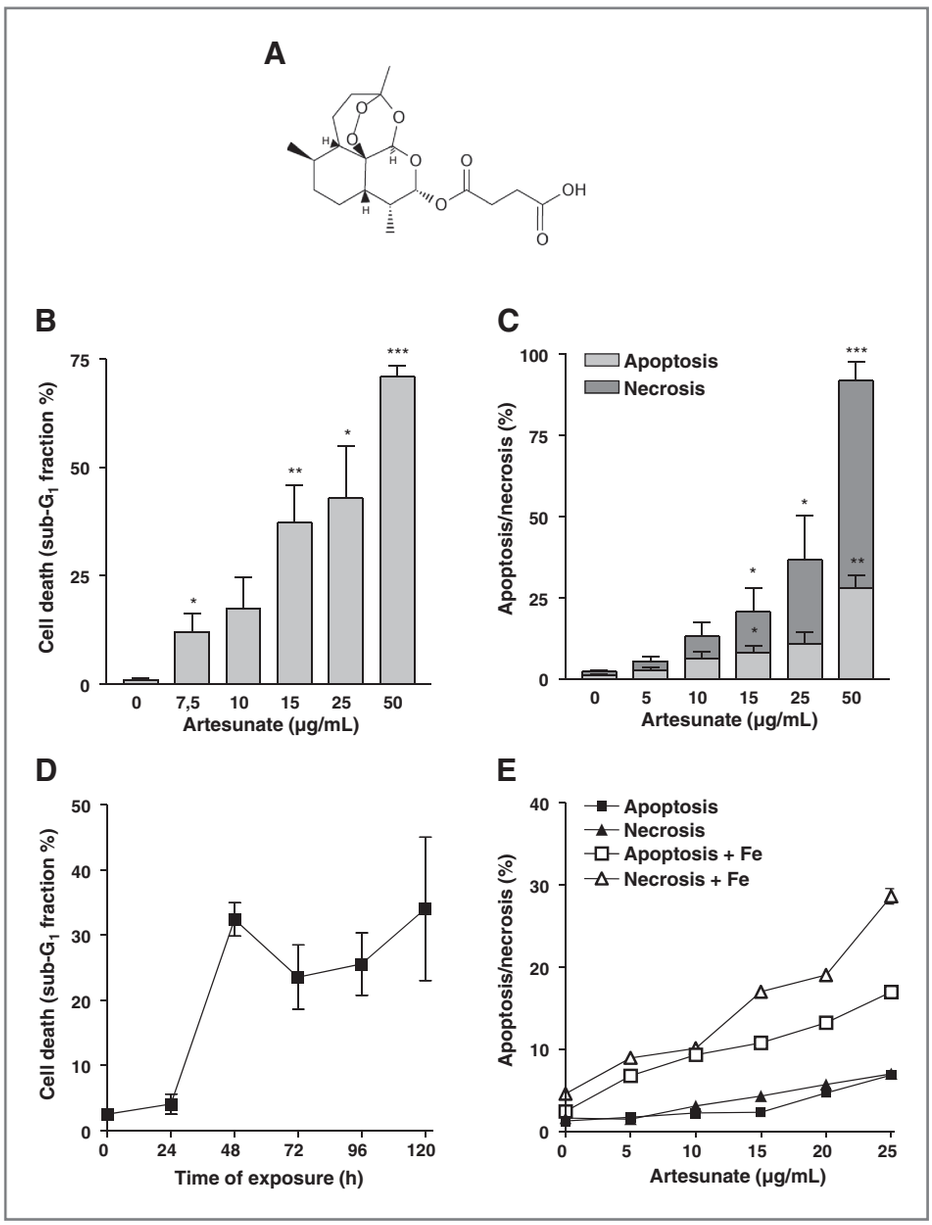

Figure 1. Cell death induced by artesunate in LN-229 glioblastoma cells. A, structural formula of artesunate. B, quantification of the sub-G_1 fraction in the cell population that was treated for 48 hours with different doses of artesunate. Cells were seeded 2 days before the onset of artesunate treatment. C, cell death (apoptosis plus necrosis) induced in LN-229 cells as measured 48 hours after artesunate treatment by Annexin V/PI double staining and flow cytometry. D, time course of induction of apoptosis, determined by sub-G_1 measurements. E, cell death (apoptosis plus necrosis) induced in LN-229 as measured by Annexin V/PI staining 48 hours after treatment with artesunate alone and artesunate together with iron (II)–glycine sulfate (10 μg/mL). All data are the mean of at least 3 independent experiments ± SD. Significance levels were compared with the nontreated control.

signaling, and apoptosis/necrosis were observed to be induced, indicating that artesunate acts as a potential genotoxic anticancer drug. The role of oxidative DNA damage was confirmed by ROS scavengers, for example, *N*-acetyl cysteine, which reversed the detrimental effects of artesunate on LN-229 cells. Hence, we were able to identify for the first time critical oxidative DNA lesions induced by artesunate in human cells that activate cell death mechanisms and thus cause cancer cell death. We also show that artesunate induces during the treatment period a sustained level of oxidative DNA lesions and DSB, which is different from ionizing radiation and that DSB repair strongly contributes to resistance of glioma cells to artesunate.

Materials and Methods

Cell culture and drug treatment

For the experiments we used the cell line LN-229, which is a human glioblastoma line wild-type for p53 (12). The line was kindly provided by Dr. M. Weller (University of Tübingen, Tübingen, Germany) and used and described in our previous work (13, 14). LN-229 cells were stably transfected with short hairpin RNA (shRNA) targeting Rad51 or with the empty vector. Selection occurred with G418 as previously described (15). We also used the cell lines MO59K and MO59J, which are isogenic human glioblastoma lines wild-type for p53, but proficient and deficient in DNA-PK_{CS}, respectively (16). The lines were a

kind gift of Dr. M. Rave-Fränk (University Medical Centre Gottingen, Göttingen, Germany) and described previously (15). Cells were cultured in Dulbecco's Modified Eagle's Medium (DMEM)/high-glucose medium supplemented with 5% fetal calf serum at 7% CO_2 and 37°C. They were cultured for a maximal period of 3 month and then replaced by a new batch. They were checked routinely for mycoplasma contamination. Artesunate (Dafra Pharma) was prepared by dissolving the drug in dimethyl sulfoxide and diluting it in sterile PBS to a final concentration of 2 mg/mL. Stock solution was aliquoted and stored at −20°C until use. Iron(II)–glycine sulfate (Ferrosanol) was obtained from Sanol and used at a concentration of 10 μg/mL. t-Butyl hydroperoxide (t-BOOH) was from Sigma and diluted in PBS.

Determination of apoptosis and necrosis

The apoptotic frequency was determined by sub-G_1 fraction or Annexin V/propidium iodide (PI) double staining quantified by flow cytometry with a FACSCalibur as previously described (17). The number of apoptotic cells and the cell populations were calculated with the CellQuestPro program of Becton Dickinson.

Determination of ROS formation

To evaluate ROS production following artesunate treatment, the membrane permeable indicator H_2DCFDA was used. Cells were preincubated with 10 μmol H_2DCFDA in serum-free medium at 37°C for 30 minutes and thereafter treated with artesunate. After different times, cells were washed twice with PBS and monitored with a FACSCalibur (Becton Dickinson) at an excitation wavelength of 488 nm and an emission wavelength of 525 nm. The ROS level was determined by comparing the changes in fluorescence intensity with that of the control.

Single-cell gel electrophoresis (comet assay)

Exponentially growing cells were exposed to artesunate and after different time periods trypsinized and washed with ice-cold PBS. Alkaline cell lysis and electrophoresis was essentially carried out as described previously (18). Formamidopyrimidine DNA glycosylase (FPG; generous gift from Bernd Epe, University of Mainz, Mainz, Germany) was added to the agarose gel on the slide at a dilution of 1 mg/mL. The slides were incubated for 45 minutes at 37°C. Electrophoresis (23 V) was carried out at 4°C for 15 minutes in 90 mmol/L Tris, 90 mmol/L boric acid, and 2 mmol/L EDTA (pH 7.5). PI-stained slides were evaluated with a fluorescence microscope and the Komet 4.0.2 software from Kinetic Imaging Ltd. Data were expressed as tail moment, which represents the percentage of DNA in the tail multiplied by the length between the centre of the head and tail (19).

Phospho-H2AX and 53BP1 immunofluorescence staining

LN-229 cells were seeded on cover slips. Following treatment with artesunate or with ionising radiation (2 Gy), cells were fixed with 4% formaldehyde at different time points. Cover slips were then blocked with 5% bovine serum albumin in PBS containing 0.3% Triton X-100. The antibodies used were monoclonal anti-γH2AX (Millipore) and/or anti-53BP1 (Millipore GmbH) and Alexa Fluor 488 (Invitrogen) or Cy3 (Abcam). Before mounting, DNA was stained with 1 μmol/L TO-PRO-3 for 15 minutes. Between all staining steps, cells on the cover slips were washed 3 times in PBS containing 0.3% Triton X-100 for 5 minutes. Slides were mounted in antifade medium (Glycerol:PBS 1:1, 2.5% DABCO, pH 8.6 with HCl) and scored with a laser scanning microscope (LSM 710) and the ZEN Software from Carl Zeiss.

8-OxoG and ethenoA immunofluorescence staining

LN-229 cells were seeded on cover slips. Following treatment with artesunate, cells were fixed with methanol:acetone (7:3) for 7 minutes at −20°C and rehydrated in PBS. After treatment with RNase A (200 μg/mL in PBS) and RNase T1 (50 units/mL in PBS) for 1 hour at 37°C, cover slips were washed in PBS. DNA was denatured by incubation in a solution containing 70 mmol/L NaOH, 0.14 mol/L NaCl, and 40% methanol for 5 minutes at 0°C. For proteolysis, cells were incubated with PBS containing 0.1% trypsine for 30 seconds followed by incubation with proteinase K (2 mg/mL in 20 mmol/L Tris/HCl and 2 mmol/L $CaCl_2$) for 10 minutes at 37°C. To avoid nonspecific antibody binding, cells were first incubated with PBS containing 1% casein for 30 minutes at room temperature and then with a rabbit anti-8-oxoG antibody or a mouse anti-ethenoA antibody (0.5 mg antibody/mL PBS containing 1% casein; (Squarix Biotechnology) for 16 hours at 4°C. Unbound antibodies were removed by extensive washing with PBS containing 0.05% Tween 20. Cy3 goat anti-rabbit or anti-mouse (2 mg/mL in PBS containing 1% bovine serum albumin; Jackson ImmunoResearch Europe Ltd.) were added for 1 hour at 37°C. After washing with PBS, nuclear DNA was stained with TO-PRO-3 (Invitrogen; 1 μmol/L in PBS). Samples were then mounted in an antifade medium (glycerol:PBS 1:1, 2.5% DABCO, pH 8.6 with HCl) and kept in the dark until microscopic analysis.

Image analysis

Fluorescence images were recorded and quantified with a laser scanning microscope (LSM 710) and the ZEN Software from Carl Zeiss AG. Each value represents the average fluorescence intensity of at least 50 nuclei.

Preparation of protein extracts and Western blot analysis

Whole-cell extracts were prepared by lysis of the cells on the plates in 95°C preheated with 1× loading buffer (Roti-Load 1; Roth). For preparing whole-cell extracts for the other Western blot analyses, cells were washed in ice-cold PBS, harvested, and resuspended in whole-cell extract buffer [20 mmol/L Tris-HCl; pH 8.5, 1 mmol/L EDTA, 1 μmol/L β-mercaptoethanol, 5% glycerol, 10 mmol/L dichlorodiphenyltrichloroethane (DDT),

0.5 mmol/L phenylmethylsulfonylfluoride (PMSF), 1 mmol/L Na_3VO_4, and proteinase inhibitor]. After sonication on ice (2 cycles of 10 pulses) with a Branson Sonifier (Cell Disruptor B15; output control = 4, 40% duty cycle), homogenates were stored at −20°C. Western blot analysis was conducted as previously described (20). Protein–antibody complexes were visualized by ECL (Amersham). Antibodies were purchased from Amersham Biosciences AB, Millipore GmbH, Calbiochem, Merck Chemicals Ltd., and Cell Signaling Technology.

Statistics

Experiments were conducted at least 3 times. Values were compared statistically using the unpaired *t* test. Significance levels were *, $P < 0.05$; **, $P < 0.005$; and ***, $P < 0.001$.

Results

Artesunate induces apoptosis and necrosis in human glioma cells

Experiments were carried out with LN-229 human glioblastoma cells, which are wild-type for p53 (14). In previous studies, we showed that these cells are repair competent and undergo apoptosis upon genotoxic anticancer drug treatment (15). Following artesunate exposure, LN-229 cells undergo apoptosis dose dependently. In the range of 5 to 50 μg/mL (chronic exposure), artesunate induces apoptosis, as determined by sub-G_1 fraction (Fig. 1B). Using Annexin V/PI double staining, we quantified the level of apoptosis and necrosis and observed that artesunate also induces a considerable amount of necrosis (Fig. 1C). Cell death by apoptosis is a late response that starts 2 days after the onset of treatment and remains at a high level for at least 5 days (Fig. 1D). The addition of Ferrosanol to the medium significantly ameliorated the frequency of apoptosis and necrosis (Fig. 1E), supporting the paradigm that a Fenton-type reaction that gives rise to ROS formation is involved in artesunate activation in cancer cells.

Artesunate induces oxidative DNA damage

To elucidate the role of ROS in artesunate-induced cell death, we determined the intracellular ROS level by H_2DCFDA staining (Fig. 2A for a representative example). Intracellular ROS clearly increased with artesunate exposure time, reaching a level after 24 hours exposure (15 μg/mL) that even exceeded the level induced by t-BOOH, which is a powerful oxidative genotoxin (Fig. 2B).

Intracellular ROS is thought to damage the nuclear DNA. Therefore, we determined the level of 8-oxoG, which is the major DNA oxidation product. We used a modified alkaline comet assay, which is based on treatment of lysed cells with FPG protein before electrophoresis. FPG is a bacterial damage–specific DNA glycosylase that recognizes 8-oxoG, and by removing the base, FPG generates apurinic sites that are converted to single-strand breaks (SSB) by the AP lyase activity of the same enzyme. As shown in Fig. 2C, in the absence of FPG, no SSB were induced, whereas in the presence of FPG, SSB were induced that increased significantly as a function of artesunate dose. These breaks were not immediately induced at significant amounts. They were first detected 6 hours after the addition of artesunate to the medium and later on remained at a high level (Fig. 2D), which indicates that DNA base damage formation by artesunate is a slow process, not comparable with direct oxidizing agents such as t-BOOH, for which 8-oxoG formation can be observed immediately after treatment (Fig. 3A).

To confirm these data, we determined the 8-oxoG levels by immunocytochemistry. As shown in Fig. 3A (for representative cytochemistry) and Fig. 3B (for quantification), artesunate clearly induces 8-oxoG immunoreactive cells. Similar to the data obtained with the FPG comet assay, 8-oxoG formation was not significantly enhanced in the first hours after addition of artesunate to the medium. It started to increase significantly only 6 hours following treatment. Interestingly, the 8-oxoG level determined after an exposure period of 24 hours was not higher than after 6 and 8 hours, indicating that an equilibrium is reached between the formation of 8-oxoG and its removal by DNA repair. Removal of 8-oxoG from DNA in the postexposure period does occur as shown in Fig. 3C. It shows that in LN-229 cells treated for 24 hours with artesunate 8-oxoG is removed from the DNA in a time-dependent manner reaching control levels 6 hours after exposure. Overall, these data support the view that artesunate in the exposure period produces a dose-dependent level of ROS that continuously attack DNA, reaching an equilibrium level that is likely determined by the concentration of artesunate in the medium and the 8-oxoG repair capacity of the cell.

Another biologically relevant DNA oxidation product is ethenoA. Because ethenoA is supposed to be a replication-blocking DNA adduct (21) and, therefore, a presumptive cytotoxic DNA lesion (22), we wondered whether artesunate is able to induce this type of DNA damage as well. LN-229 cells treated with artesunate (15 μg/mL) clearly showed the formation of ethenoA, as shown by immunostaining that increased with treatment time (Fig. 4A). Quantification revealed that after 6 hours the level was significantly enhanced and 24 hours following treatment an ethenoA level similar to a toxic dose (400 mmol/L) of t-BOOH was reached (Fig. 4B). The finding substantiates that artesunate generates a sustained ROS level that continuously induces oxidative DNA damage and that this damage accumulates over the treatment period.

If artesunate generates DNA-damaging ROS in mammalian cells, it is anticipated that ROS scavengers are able to reduce the level of DNA damage. This was indeed the case as curcumin, resveratrol, and *N*-acetyl cysteine, all of which have radical scavenging properties (23–26), completely prevented artesunate-mediated 8-oxoG formation (Fig. 4C). Furthermore, the ROS scavenger *N*-acetyl cysteine greatly reduced the killing effect of artesunate in LN-229 cells (Fig. 4D), indicating that

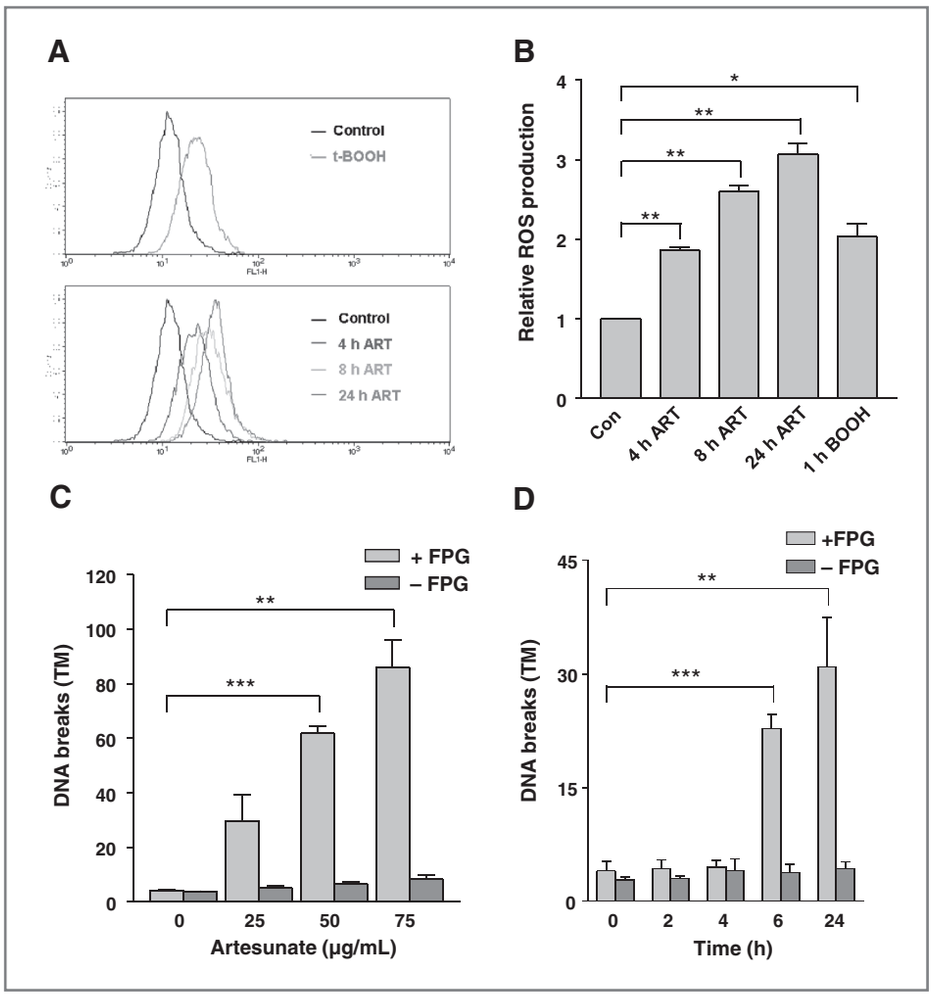

Figure 2. Formation of ROS and induction of FPG-sensitive sites by artesunate. A, chloromethyl-H_2DCFDA staining, an indicator for ROS formation, determined by fluorescence-activated cell sorting at different time points after treatment with 15 μg/mL artesunate (ART); 1-hour treatment with t-BOOH was used as a positive control. B, relative ROS production measured at different time points after treatment with 15 μg/mL artesunate (ART); t-BOOH was used as a positive control (Con). C, FPG-sensitive sites induced by artesunate. LN-229 cells were exposed to artesunate with different doses for 24 hours, harvested, embedded in agarose, lysed, incubated in the presence and absence of FPG protein, and subjected to alkaline single-cell gel electrophoresis. TM, tail moment. D, cells were treated with a concentration of 25 μg/mL artesunate and harvested at the indicated time points. Cells were subjected to alkaline single-cell gel electrophoresis as described earlier in the presence or absence of FPG protein. Data are the mean of at least 3 independent experiments ± SD. TM, tail moment.

artesunate-induced oxidative DNA damage is responsible for the killing effect of the drug.

Artesunate induces a sustained increasing level of DNA DSBs, which is different from ionizing radiation

The most severe lethal lesions produced by ROS are DSB (27), which are powerful inducer of apoptosis (28). To elucidate whether artesunate is able to induce DSB, we determined the phosphorylation level of histone 2AX (γH2AX). As shown in Fig. 5A, H2AX phosphorylation at ser139 occurred already 2 hours after the onset of artesunate treatment, increased with time 6 hours later, and remained at this high level up to 24 hours following treatment. We also determined γH2AX foci by immunocytochemistry (Fig. 5B for a representative example and Fig. 5C for quantification), which is a widely accepted marker for DSB (29, 30). As shown in a dose-dependent experiment in Fig. 5D, artesunate induces γH2AX foci in LN-229 cells that increased nearly linearly with exposure time, which is in stark contrast to ionizing radiation for which γH2AX foci reached a maximum 1 hour after treatment and thereafter declined (Fig. 5D) as a result of DSB repair (31). In artesunate-exposed cells, a maximum level was induced at 10 hours that did not increase further when the exposure time was extended to 24 hours (Fig. 5D), which is conform with the hypothesis that DSB are formed and repaired leading finally to an equilibrium level in the artesunate exposure period. γH2AX foci colocalized with 53BP1 (Fig. 5E for a representative example and Fig. 5F for quantification), which is a strong additional indication for the ability of artesunate to induce "true" DSB.

Both homologous recombination and nonhomologous end joining protect against artesunate-induced cell death

Previously, we reported that mutant Chinese hamster cells impaired in the homologous recombination (HR) pathway of DSB repair are hypersensitive to artesunate (11). This finding prompted us to translate the finding to cancer cells and determined whether downregulation of HR in glioma LN-229 cells impacts their killing response following artesunate treatment. To this end, we stably

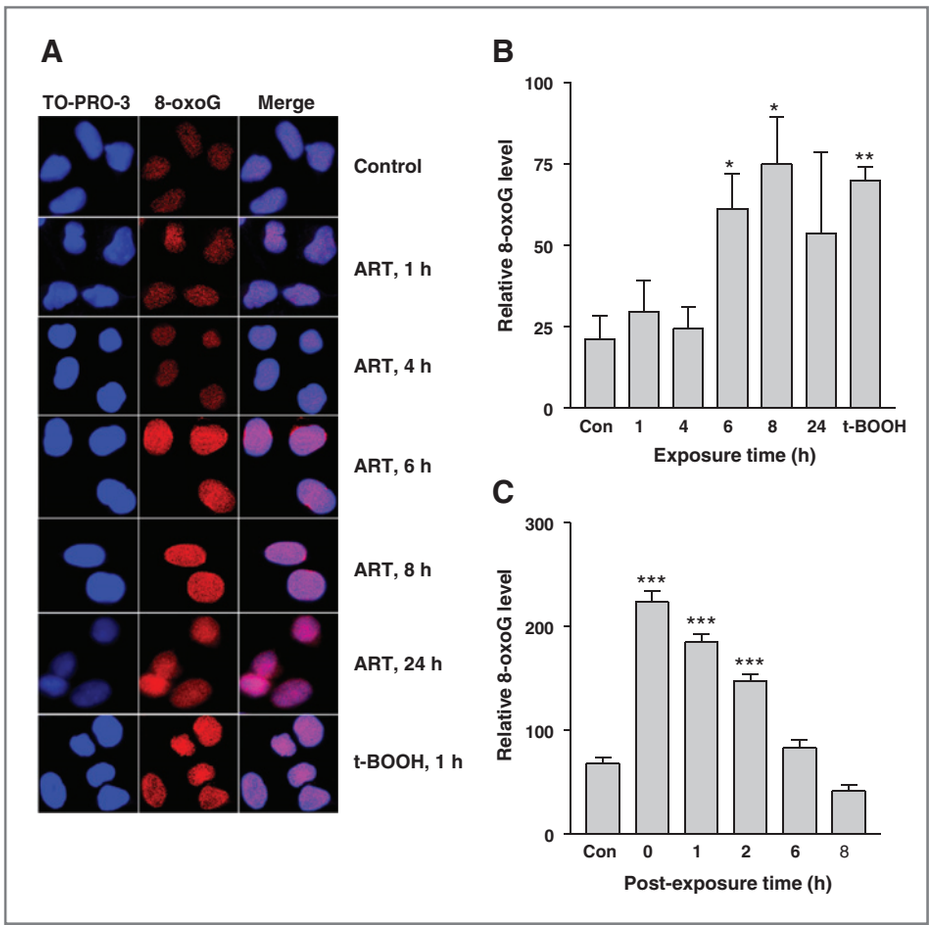

Figure 3. Formation of 8-oxoG following artesunate treatment of LN-229 glioblastoma cells. A, immunofluorescence staining of 8-oxoG after artesunate (15 μg/mL) at different times of exposure; t-BOOH (400 mmol/L, 1-hour treatment) was used as a positive control. The negative control was only treated with the secondary antibody (not shown). TO-PRO-3, nuclear staining. B, the 8-oxoG level was measured by quantifying the fluorescence intensity with LSM and the appropriate Zeiss software. C, 8-oxoG level as a function of time following artesunate treatment. Exponentially growing LN-229 cells were treated with artesunate for 24 hours. The medium was replaced, and cells were harvested for 8-oxoG staining at indicated times postexposure. The fluorescence intensity was determined with LSM software. Al least 50 cells were counted per experiment and measure point. Data are the mean of 3 independent experiments ± SD.

transfected LN-229 cells with a Rad51 shRNA vector, which clearly downregulates Rad51 protein expression (Fig. 6A, insert). Treatment of these cells with artesunate led to a dramatic increase in the level of apoptosis as compared with empty vector–transfected cells (Fig. 6A). These data substantiate our previous finding that the HR repair pathway is involved in protection against artesunate-induced genotoxicity.

Is nonhomologous end joining (NHEJ) involved in DSB repair following artesunate treatment as well? To this end, we assessed the killing response of a pair of glioma cells wild-type (MO59K) and mutated for DNA-PK_{CS} (MO59J). MO59K cells were highly resistant to artesunate and underwent cell death (executed mostly by necrosis) only at the high-dose level of 50 μg/mL (Fig. 6B). In contrast, MO59J cells were more sensitive, undergoing death already at 10 μg/mL artesunate (Fig. 6C). In these cells, death was executed mostly by apoptosis and less by necrosis (compare Fig. 6B and C). To substantiate that NHEJ is involved in protection against artesunate, we treated p53 wild-type glioma cells (LN-229) with a DNA-PK_{CS} inhibitor (NU7026). Inhibition of DNA-PK_{CS}, which is a main component of NHEJ, greatly sensitized glioma cells to artesunate (Fig. 6D, compare with Fig. 1C). Similar to MO59K cells, a large amount of necrosis was induced (Fig. 6D). This necrosis induction is related to ATP depletion, which is currently under study (data not shown). These data suggest that NHEJ, together with HR, is involved in the defense against artesunate-induced DNA damage.

Artesunate induces the DNA damage response

As shown in Fig. 6E, artesunate treatment of LN-229 glioma cells gives rise to a dose-dependent increase in the level of phosphorylated ATM, ATR, Chk2, and Chk1, which was determined 8 hours after the onset of treatment. The data are conform with the notion that artesunate generates oxidative DNA damage, yielding DSB that trigger activation of the ATM/ATR/Chk1/Chk2 damage response pathway.

Discussion

This study was conducted to provide evidence that artesunate, which is a widely used drug for the treatment of malaria, is able to induce oxidative DNA damage in mammalian cells. We used a glioma cell line (LN-229) for the study because the mechanism of death in glioma cells

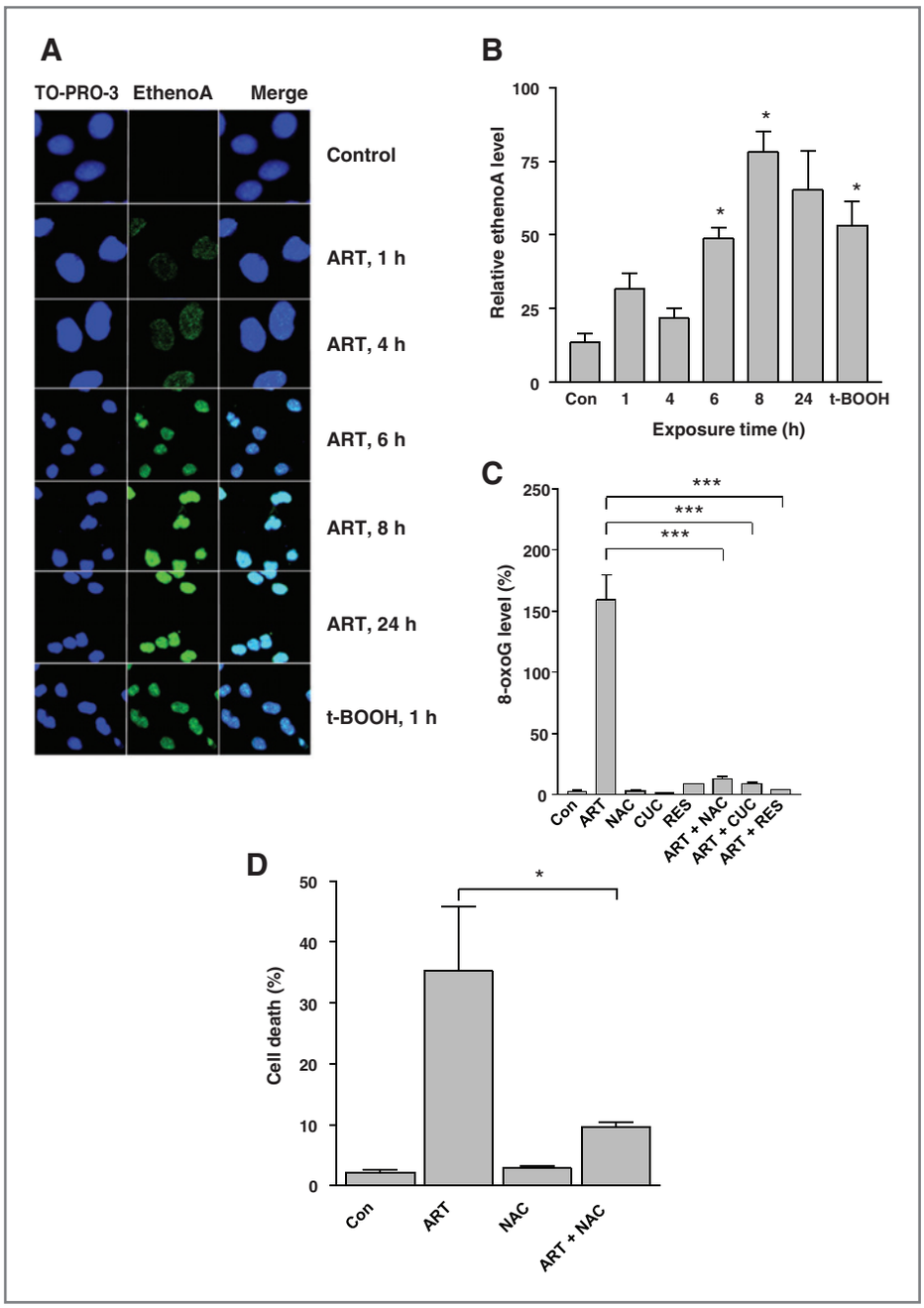

Figure 4. Induction by artesunate of ethenoA in LN-229 glioblastoma cells and effect of radical scavengers. A, immunofluorescence staining of ethenoA after artesunate (15 μg/mL) at different times following treatment; t-BOOH (400 mmol/L, 1-hour treatment) was used as positive control. B, the ethenoA level was measured by quantifying the fluorescence intensity with LSM and the ZEN software. C, effects of radical scavenger on artesuante-induced death in LN-229 cells. Cells were incubated with different radical scavengers, *N*-acetyl cysteine (NAC, 10 mmol/L), curcumin (CUC, 5 mmol/L), and resveratrol (RES, 5 mmol/L), in the presence and absence of artesunate (15 μg/mL). The intensity of ethenoA was measured by quantifying the fluorescence intensity with LSM. D, effect of NAC on artesunate-induced cell death. Cells were incubated with either the radical scavenger *N*-acetyl cysteine (NAC, 10 mmol/L), ART (15 μg/mL), or with the combination of both agents (ART 15 μg/mL + NAC 10 mmol/L), and cell death was measured 48 hours after treatment by Annexin V/PI staining and fluorescence-activated cell sorting. Experiments were carried out 3 times. Data in B show a representative experiment (50 cells counted ± SD).

following DNA damage has been well established in our previous work (13–15). Here, we show for the first time that artesunate is able to induce 8-oxoG and ethenoA, which are 2 main oxidative DNA base adducts. We should note that 8-oxoG is a mispairing lesion that is considered to be responsible for the induction of point mutations following ROS (32–34). This points to the possibility that artesunate bears a mutagenic potential, which should be considered a side effect of its use as an antimalaria drug. EthenoA is likely a replication-blocking lesion (21, 22) that, if not repaired in time, may cause stalled DNA replication that ends up with DSB formation and activation of the DNA damage response (DDR). This was indeed observed in LN-229 glioma cells. Our observation that downregulation of HR (by siRad51) greatly ameliorates the killing effect of artesunate is compatible with the model that stalled and finally collapsed replication forks yield the formation of DSB that finally trigger apoptosis (35). Artesunate-induced ROS may also produce DSB directly. This minor fraction is, similar to ionizing

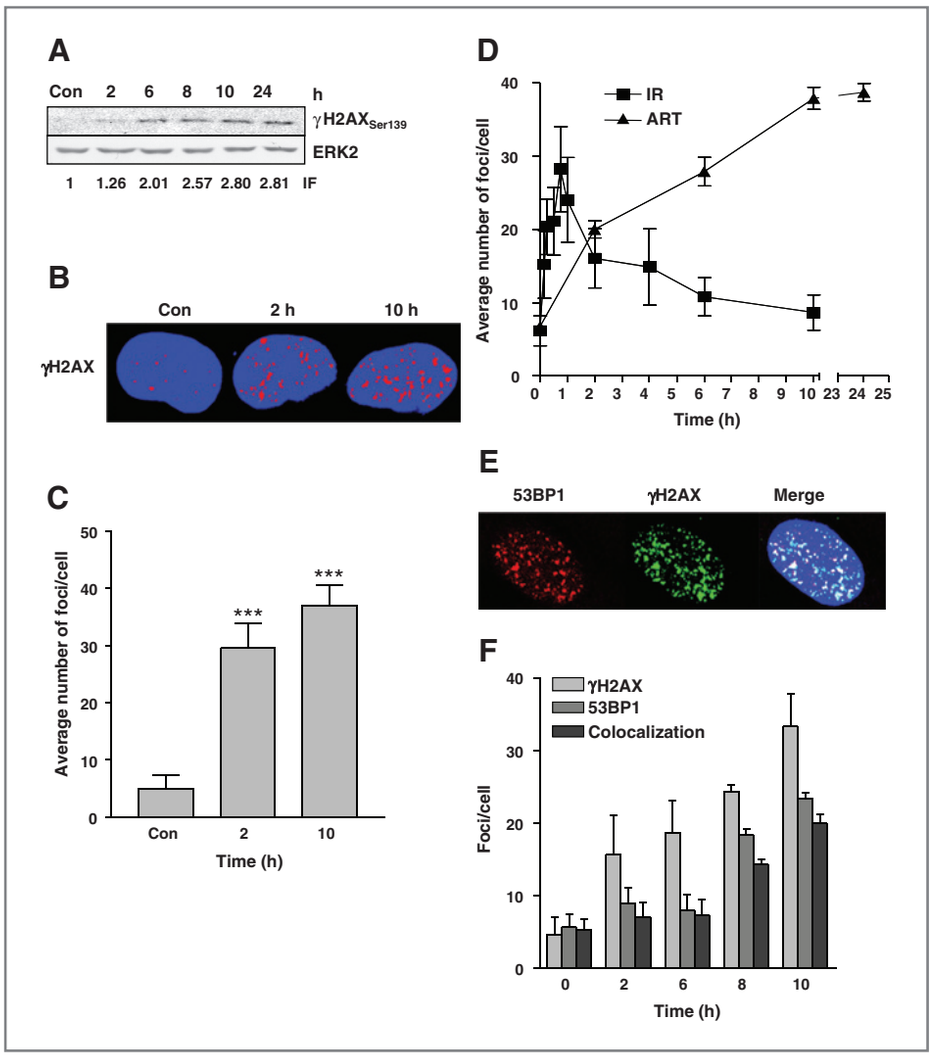

Figure 5. Level of γH2AX and 53BP1 following artesunate treatment. A, exponentially growing LN-229 cells were exposed to artesunate up to 24 hours, harvested, and subjected to Western blot analysis. As loading control, the filter was reincubated with extracellular signal–regulated kinase 2 (ERK2). IF, induction factor (γH2AX/ERK2 in relation to the control). B, representative example of γH2AX nuclear foci and the average number of foci per cell (C) after ART treatment (15 μg/mL) of LN-229 cells. D, number of γH2AX foci per LN-229 cell after treatment with γ-rays (2 Gy) and with 15 μg/mL artesunate. Cells were in the exponentially growth phase and irradiated at zero time. Artesunate was added to the medium at zero time and left there until cells were harvested at the indicated times. Data are the mean of 3 independent experiments ± SD. E, colocalization of γH2AX and 53BP1, showing a representative example, and the average number of foci per cell (F) after artesunate treatment (15 μg/mL). IR, ionizing radiation.

radiation (36), likely to be subject to NHEJ, which explains why both HR and NHEJ are significantly involved in the defense against artesunate-induced DNA damage. The finding that artesunate activates ATM/Chk2 and ATR/Chk1 supports the hypothesis that directly induced and replication-mediated DSB contribute to the genotoxic and killing responses observed.

It is striking that following treatment with artesunate, oxidative lesions and DSBs are not formed immediately at high amount but slowly accumulate until a saturation level is reached. This is in contrast to the well-known effect of ionizing radiation that induces a burst of DSB immediately after irradiation (Fig. 5D; see also ref. 37). Interestingly, the frequency of DSB (as determined by phosphorylation of ser139 of H2AX) following artesunate increased with time after exposure reaching a plateau, which is explained by the equilibrium between the formation and repair of DNA lesions. Thus, although artesunate is a ROS producer, it differs significantly from ionizing radiation and chemical oxidative agents in their ability to produce a sustained level of oxidative DNA lesions including DSB. Chronic and sustained formation of low-level DNA adducts and DSB that accumulate in the treatment period is not achieved by acute radiation and chemical direct oxidizing agents. We hypothesize that the sustained formation of DNA oxidation products, notably DSB, following artesunate may differ in their biological consequences from lesions that are formed in a pulse-wise manner being, if generated above a particular threshold level, an activator of death signaling, which is supposed to be tolerated in normal but not tumor cells.

Another reasonable supposition for tumor specificity of the killing effect of artesunate rests on artesunate activation by ferrous iron, which gained support by our experiments with Ferrosanol that strongly enhanced the killing effect of artesunate in LN-229 glioma cells. Because tumors frequently overexpress iron transporter, a tumor specificity of artesunate-induced cell kill is anticipated. The finding that the cytotoxic effect of artesunate in human cells is due to ROS-induced DSBs, which are

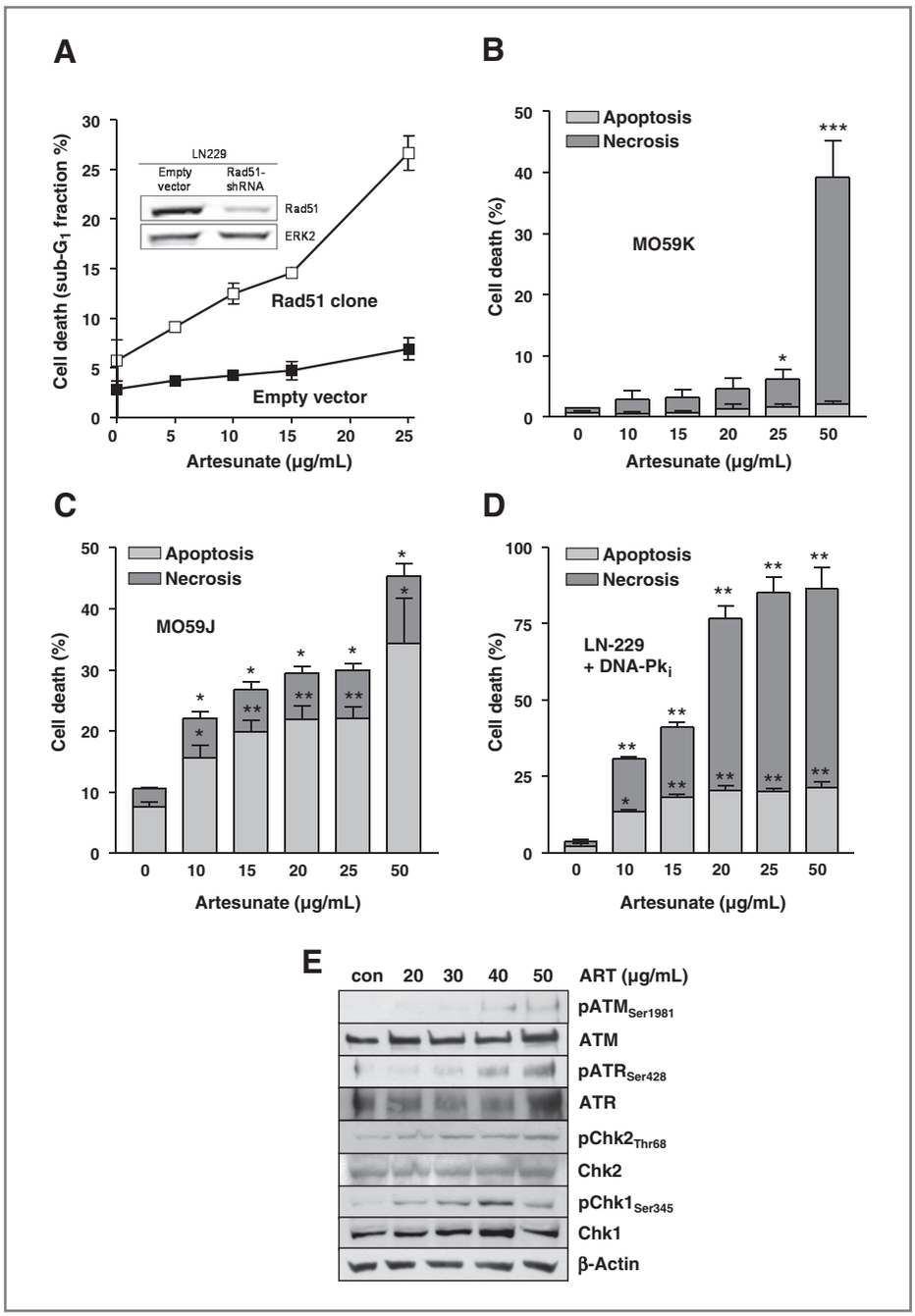

Figure 6. Artesunate-induced glioma cell death in Rad51 downregulated and DNA-PK_{CS}–mutated cells as well as phosphorylation of players of the DDR. A, LN-229 cells were stably transfected with shRNA targeting Rad51 or with empty vector, and induced cell death (apoptosis plus necrosis) was determined 48 hours after treatment with different doses of artesunate by Annexin V/PI flow cytometry. Inset, the efficiency of Rad51 knockdown was tested by Western blot analysis. As loading control, the filter was reincubated with ERK2. B, artesunate-induced death (the sum of apoptosis and necrosis determined by Annexin V/PI flow cytometry) in DNA-PK_{CS} wild-type glioma MO59K cells and DNA-PK_{CS} MO59J mutant cells (C). D, effect of the DNA-PK inhibitor (DNA-PK_i) NU7026 on death of artesunate-treated LN-229 cells. Cells were treated with the inhibitor (10 μmol/L) 2 hours before the addition of artesunate to the medium. E, phosphorylation of ATM, ATR, Chk2, and Chk1 in LN-229 cells after artesunate treatment, which was determined 8 hours after the onset of treatment. To verify equal protein levels, the total amount of nonphosphorylated proteins and β-actin was determined.

repaired by HR and NHEJ, may open up strategies for the inclusion of artesunate in cancer therapy protocols.

In our experiments, we observed DSB formation and activation of DDR within the artesunate treatment period much earlier than the onset of apoptosis. This lag phase between the induction of critical lesions and apoptosis execution is also known from other experimental systems and genotoxic exposures (15, 28). It is tempting to speculate that critical components of the cell death pathway need to become accumulated until the pathway can be fully activated. We should also note that compared with other genotoxic anticancer drugs such as temozolomide artesunate induces a comparatively high level of necrosis. This could be the consequence of extensive base damage that activates base excision repair, which in turn leads to ATP depletion. Because apoptosis requires ATP (33), the necrotic pathway will be activated. Work is in progress to clarify this question.

Disclosure of Potential Conflicts of Interest

No potential conflicts of interest were disclosed.

Acknowledgments

The authors thank Dr. Herwig Jansen (Dafra Pharma) for a gift of artesunate, Prof. Bernd Epe for FPG protein, and Anna Frumkina for her help with the comet assays.

Grant Support

This work was supported by a grant from the University of Mainz.

The costs of publication of this article were defrayed in part by the payment of page charges. This article must therefore be hereby marked *advertisement* in accordance with 18 U.S.C. Section 1734 solely to indicate this fact.

Received July 19, 2011; revised September 28, 2011; accepted October 3, 2011; published OnlineFirst October 13, 2011.

References

1. Dell'Eva R, Pfeffer U, Vene R, Anfosso L, Forlani A, Albini A, et al. Inhibition of angiogenesis *in vivo* and growth of Kaposi's sarcoma xenograft tumors by the anti-malarial artesunate. Biochem Pharmacol 2004;68:2359–66.
2. Efferth T. Mechanistic perspectives for 1,2,4-trioxanes in anti-cancer therapy. Drug Resist Updat 2005;8:85–97.
3. Efferth T, Dunstan H, Sauerbrey A, Miyachi H, Chitambar CR. The anti-malarial artesunate is also active against cancer. Int J Oncol 2001; 18:767–73.
4. Berman PA, Adams PA. Artemisinin enhances heme-catalysed oxidation of lipid membranes. Free Radic Biol Med 1997;22:1283–8.
5. Meshnick SR, Yang YZ, Lima V, Kuypers F, Kamchonwongpaisan S, Yuthavong Y. Iron-dependent free radical generation from the anti-malarial agent artemisinin (qinghaosu). Antimicrob Agents Chemother 1993;37:1108–14.
6. Asawamahasakda W, Ittarat I, Pu YM, Ziffer H, Meshnick SR. Reaction of antimalarial endoperoxides with specific parasite proteins. Antimicrob Agents Chemother 1994;38:1854–8.
7. Eckstein-Ludwig U, Webb RJ, Van Goethem ID, East JM, Lee AG, Kimura M, et al. Artemisinins target the SERCA of *Plasmodium falciparum*. Nature 2003;424:957–61.
8. Efferth T, Benakis A, Romero MR, Tomicic M, Rauh R, Steinbach D, et al. Enhancement of cytotoxicity of artemisinins toward cancer cells by ferrous iron. Free Radic Biol Med 2004;37:998–1009.
9. Kelter G, Steinbach D, Konkimalla VB, Tahara T, Taketani S, Fiebig HH, et al. Role of transferrin receptor and the ABC transporters ABCB6 and ABCB7 for resistance and differentiation of tumor cells towards artesunate. PLoS One 2007;2:e798.
10. Efferth T, Kaina B. Toxicity of the antimalarial artemisinin and its dervatives. Crit Rev Toxicol 2010;40:405–21.
11. Li PC, Lam E, Roos WP, Zdzienicka MZ, Kaina B, Efferth T. Artesunate derived from traditional Chinese medicine induces DNA damage and repair. Cancer Res 2008;68:4347–51.
12. Weller M, Rieger J, Grimmel C, Van Meir EG, De Tribolet N, Krajewski S, et al. Predicting chemoresistance in human malignant glioma cells: the role of molecular genetic analyses. Int J Cancer 1998;79:640–4.
13. Batista LF, Roos WP, Christmann M, Menck CF, Kaina B. Differential sensitivity of malignant glioma cells to methylating and chloroethylating anticancer drugs: p53 determines the switch by regulating xpc, ddb2, and DNA double-strand breaks. Cancer Res 2007;67:11886–95.
14. Hermisson M, Klumpp A, Wick W, Wischhusen J, Nagel G, Roos W, et al. O6-methylguanine DNA methyltransferase and p53 status predict temozolomide sensitivity in human malignant glioma cells. J Neurochem 2006;96:766–76.
15. Roos WP, Batista LF, Naumann SC, Wick W, Weller M, Menck CF, et al. Apoptosis in malignant glioma cells triggered by the temozolomide-induced DNA lesion O6-methylguanine. Oncogene 2007;26:186–97.
16. Allalunis-Turner MJ, Zia PK, Barron GM, Mirzayans R, Day RS III. Radiation-induced DNA damage and repair in cells of a radiosensitive human malignant glioma cell line. Radiat Res 1995;144:288–93.
17. Naumann SC, Roos WP, Jost E, Belohlavek C, Lennerz V, Schmidt CW, et al. Temozolomide- and fotemustine-induced apoptosis in human malignant melanoma cells: response related to MGMT, MMR, DSBs, and p53. Br J Cancer 2009;100:322–33.
18. Christmann M, Tomicic MT, Gestrich C, Roos WP, Bohr VA, Kaina B. WRN protects against topo I but not topo II inhibitors by preventing DNA break formation. DNA Repair (Amst) 2008;7:1999–2009.
19. Olive PL, Banath JP, Durand RE. Heterogeneity in radiation-induced DNA damage and repair in tumor and normal cells measured using the "comet" assay. Radiat Res 1990;122:86–94.
20. Renart J, Reiser J, Stark GR. Transfer of proteins from gels to diazobenzyloxymethyl-paper and detection with antisera: a method for studying antibody specificity and antigen structure. Proc Natl Acad Sci U S A 1979;76:3116–20.
21. Pourquier P, Bjornsti MA, Pommier Y. Induction of topoisomerase I cleavage complexes by the vinyl chloride adduct 1,*N*6-ethenoadenine. J Biol Chem 1998;273:27245–9.
22. Basu AK, Wood ML, Niedernhofer LJ, Ramos LA, Essigmann JM. Mutagenic and genotoxic effects of three vinyl chloride-induced DNA lesions: 1,*N*6-ethenoadenine, 3,*N*4-ethenocytosine, and 4-amino-5-(imidazol-2-yl)imidazole. Biochemistry 1993;32:12793–801.
23. Hatcher H, Planalp R, Cho J, Torti FM, Torti SV. Curcumin: from ancient medicine to current clinical trials. Cell Mol Life Sci 2008;65:1631–52.
24. Kawamori T, Lubet R, Steele VE, Kelloff GJ, Kaskey RB, Rao CV, et al. Chemopreventive effect of curcumin, a naturally occurring anti-inflammatory agent, during the promotion/progression stages of colon cancer. Cancer Res 1999;59:597–601.
25. Lim GP, Chu T, Yang F, Beech W, Frautschy SA, Cole GM. The curry spice curcumin reduces oxidative damage and amyloid pathology in an Alzheimer transgenic mouse. J Neurosci 2001;21:8370–7.
26. Martin AR, Villegas I, La Casa C, de la Lastra CA. Resveratrol, a polyphenol found in grapes, suppresses oxidative damage and stimulates apoptosis during early colonic inflammation in rats. Biochem Pharmacol 2004;67:1399–410.
27. Hartwig A. The role of DNA repair in benzene-induced carcinogenesis. Chem Biol Interact 2010;184:269–72.
28. Lips J, Kaina B. DNA double-strand breaks trigger apoptosis in p53-deficient fibroblasts. Carcinogenesis 2001;22:579–85.
29. Kuo LJ, Yang LX. Gamma-H2AX - a novel biomarker for DNA double-strand breaks. In Vivo 2008;22:305–9.
30. Sedelnikova OA, Rogakou EP, Panyutin IG, Bonner WM. Quantitative detection of (125)IdU-induced DNA double-strand breaks with gamma-H2AX antibody. Radiat Res 2002;158:486–92.
31. Goodarzi AA, Jeggo P, Lobrich M. The influence of heterochromatin on DNA double strand break repair: Getting the strong, silent type to relax. DNA Repair (Amst) 2010;9:1273–82.
32. Klaunig JE, Kamendulis LM. The role of oxidative stress in carcinogenesis. Annu Rev Pharmacol Toxicol 2004;44:239–67.
33. Lindahl T, Barnes DE. Repair of endogenous DNA damage. Cold Spring Harb Symp Quant Biol 2000;65:127–33.
34. Nyaga SG, Jaruga P, Lohani A, Dizdaroglu M, Evans MK. Accumulation of oxidatively induced DNA damage in human breast cancer cell lines following treatment with hydrogen peroxide. Cell Cycle 2007;6: 1472–8.
35. Roos WP, Kaina B. DNA damage-induced cell death by apoptosis. Trends Mol Med 2006;12:440–50.
36. Jeggo P, Lobrich M. Radiation-induced DNA damage responses. Radiat Prot Dosimetry 2006;122:124–7.
37. Rothkamm K, Lobrich M. Evidence for a lack of DNA double-strand break repair in human cells exposed to very low x-ray doses. Proc Natl Acad Sci U S A 2003;100:5057–62.